Acta Crystallographica Section D
Biological Crystallography
ISSN 0907-4449

Structure of *Escherichia coli* ribonucleotide reductase R2 in space group $P6_122$

Monika Sommerhalter,[a] Lana Saleh,[b] J. Martin Bollinger Jr[b] and Amy C. Rosenzweig[a]*

[a]Departments of Biochemistry, Molecular Biology and Cell Biology and of Chemistry, Northwestern University, Evanston, IL 60208, USA, and [b]Department of Biochemistry and Molecular Biology, The Pennsylvania State University, University Park, PA 16802, USA

Correspondence e-mail: amyr@northwestern.edu

Received 22 August 2005
Accepted 20 October 2005

PDB Reference: ribonucleotide reductase R2, 2alx, r2alxsf.

A new crystal form of wild-type ribonucleotide reductase R2 from *Escherichia coli* was obtained. Crystals grow in space group $P6_122$ with one R2 monomer in the asymmetric unit. A twofold crystallographic symmetry axis generates the physiological dimeric form of R2. Co-crystallization with $CoCl_2$ or $MnCl_2$ results in full occupancy of the dinuclear metal site. The structure of the Mn^{II}-loaded form was determined to 2.6 Å resolution by molecular replacement. The crystallization conditions, backbone conformation, crystal-packing interactions and metal centers are compared with those of previously determined crystal forms.

1. Introduction

Ribonucleotide reductase (RNR) catalyzes the conversion of ribonucleotides to deoxyribonucleotides (Sjöberg, 1997; Stubbe & Donk, 1998; Eklund *et al.*, 2001). RNR is an essential enzyme in all organisms, providing the necessary precursors for DNA synthesis and repair (Reichard, 1993). Class I RNR from *Escherichia coli*, one of the best studied RNRs, consists of two subunits, the 86 kDa R1 subunit and the 43 kDa R2 subunit. R1 contains binding sites for substrates and allosteric effectors and R2 houses a catalytically essential tyrosyl radical. The reduction of ribonucleotides to deoxyribonucleotides occurs by a radical mechanism involving both subunits (Stubbe & Donk, 1998). In the R2 subunit, the tyrosyl radical is produced through the reaction of oxygen with a diiron(II) center. The tyrosyl radical is then believed to generate a thiyl radical in the R1 active site *via* electron transfer. Crystal structures of R1 (Uhlin & Eklund, 1994) and R2 (Nordlund *et al.*, 1990) have been determined separately.

The initial wild-type R2 (wt-R2) structure revealed the protein fold and details of the active site (Nordlund *et al.*, 1990; Nordlund & Eklund, 1993). In subsequent crystallographic studies, the diiron center was characterized in different oxidation states and probed through metal substitutions and point mutations (Logan *et al.*, 1996; Tong *et al.*, 1998; Andersson *et al.*, 1999; Voegtli *et al.*, 2000, 2003; Högbom *et al.*, 2001). This array of structures is accompanied by extensive kinetic and spectroscopic data (Stubbe & Donk, 1998), synthetic modeling work (Tshuva & Lippard, 2004) and theoretical calculations (Noodleman *et al.*, 2004). Notably, there are some discrepancies between the crystal structures and solution studies regarding the occupancy and coordination numbers of the diiron center (Sommerhalter *et al.*, 2005). For the diiron(II) form, circular dichroism (CD) and magnetic circular dichroism (MCD) spectroscopic data indicate the presence of one four-coordinate and one five-coordinate Fe^{II}

Table 1
Data-collection and refinement statistics.

Values in parentheses are for the highest resolution shell, which is 2.74–2.60 Å for the data-collection statistics and 2.76–2.60 Å for the refinement statistics.

Data collection	
Space group	$P6_122$
Unit-cell parameters (Å)	$a = b = 93$, $c = 201$
Wavelength (Å)	1.0000
Resolution range (Å)	20–2.60
No. of observations	110890 (16395)
No. of unique observations	16493 (2353)
Completeness (%)	99.7 (100)
Multiplicity	6.7 (7.0)
$R_{\rm merge}$ (%)	0.080 (0.383)
$I/\sigma(I)$	16.5 (4.4)
Refinement	
Resolution range (Å)	20–2.60
No. of reflections	16437
No. of reflections in test set (10%)	1647
R factor	22.7 (32.3)
$R_{\rm free}$	27.6 (38.4)
No. of atoms	2788
No. of protein atoms	2782
No. of non-protein atoms	6
R.m.s. bond length (Å)	0.007
R.m.s. bond angles (°)	1.2
Average B value, main chain (Å^2)	60.2
Average B value, side chain (Å^2)	62.0
B value for Mn1 and Mn2 (Å^2)	41.3
B value for Hg1–4 (Å^2)	61.3

ion (Pulver *et al.*, 1995). If crystals containing the diiron(III) center are chemically reduced or photoreduced, a structure with two four-coordinate Fe^{II} ions results. However, soaking apo crystals in solutions of Fe^{II} ions results in a structure more consistent with the spectroscopic data (Sommerhalter *et al.*, 2005; Voegtli *et al.*, 2003). Since these procedures for generating the diiron(II) form result in different structures, it is likely that crystallization conditions also play a role. Multiple crystal forms can help to address variations between solution and crystallographic studies and would be particularly useful for R2 since the structure of the diiron center is commonly invoked as a starting point for mechanistic speculation and computational work.

2. Materials and methods

2.1. Crystallization

The apo form of wt-R2 was purified as described previously (Moënne-Loccoz *et al.*, 1998). A starting solution of 65 mg ml^{-1} wt-R2 in 100 m*M* HEPES pH 7.6 was diluted to 10 mg ml^{-1} with ddH_2O and supplemented with 100 m*M* $MgCl_2$ and 1 m*M* sodium ethylmercurithiosalicylate (EMTS). The Classics screen from Nextal was used to screen for new crystallization conditions. 1 µl protein solution was mixed with 1 µl screen solution in 96-well sitting-drop trays and equilibrated against 100 µl screen solution in each reservoir. After several days at room temperature, soccer-ball-shaped crystals of dimensions 0.1 × 0.1 × 0.1 mm appeared in screen condition No. 33, which contains 10 m*M* $CoCl_2{\cdot}6H_2O$, 100 m*M* MES pH 6.5 and 1.8 *M* ammonium sulfate. Optimization indicated that $CoCl_2$ can be omitted or replaced with $MnCl_2$ and that the EMTS in the protein solution is optional. The buffer can be replaced with 100 m*M* HEPES pH 7.5 or 100 m*M* EPPS pH 8.2 without obvious changes in crystal quality. Addition of 50 m*M* NaF results in a change in the shape of the crystals from soccer-ball-like to spiky bipyramids with sixfold symmetry at the base (Fig. 1). Crystals are obtained at temperatures in the range 298–310 K. The crystal size was increased to 0.5 × 0.5 × 1 mm by using a sealed Petri dish with 2 ml well solution and drops containing 10 µl protein solution and 10 µl precipitant. The best cryoprotecting agent is saturated Li_2SO_4 (Rubinson *et al.*, 2000). For data collection, crystals were removed from the crystallization drop with a rayon loop, quickly dragged through the saturated Li_2SO_4 solution and flash-cooled in liquid nitrogen. Aerobic cocrystallization or soaking attempts with ferrous ammonium sulfate stabilized by sulfuric acid were not successful owing to protein precipitation and crystal deterioration.

2.2. Data collection and refinement

X-ray diffraction data were collected at 113 K at the DND-CAT and LS-CAT beamlines at the Advanced Photon Source (APS) (Table 1). The crystals diffracted at best to 2.3 Å resolution and more typically to ∼2.6 Å resolution. Here, we report the 2.6 Å resolution structure determined from a crystal grown in the presence of $MnCl_2$. Data were integrated with *MOSFLM* (Powell, 1999) or *XDS* (Kabsch, 1993) and scaled with *SCALA* (Collaborative Computational Project, Number 4, 1994). The unit-cell parameters are $a = b = 93$, $c = 201$ Å and the space group was determined to be either $P6_1$, $P6_5$, $P6_122$ or $P6_522$. Molecular replacement using the program *MOLREP* (Vagin & Teplyakov, 1997) was successful for $P6_122$. The best solution, obtained using the structure of diiron(II) R2 at neutral pH (PDB code 1piy) without solvent molecules or metal ions as a starting model, had an R factor of 0.450 and a correlation coefficient of 0.629.

Initial rigid-body refinement with the program *REFMAC* (Murshudov *et al.*, 1997) was followed by iterative cycles of energy minimization, simulated annealing and grouped B-factor refinement with *CNS* (Brünger *et al.*, 1998). Model inspection and manual rebuilding were performed using *XtalView* (McRee, 1999). The structure was systematically examined with simulated-annealing omit maps, omitting 5–10% of the model at a time. The positions of metal ions were determined from $F_o - F_c$ difference maps and Lennard–Jones parameters for Mn^{II} were used. To determine the occupancy of the metal sites, the Mn^{II} ion B factors were fixed to a value of 41.3 Å^2, which is close to the B factor of the surrounding amino acids. Refinement of the metal occupancies resulted in values of 1.0. Fixing the occupancy of the metal sites to 1.0 also yields reasonable refined B factors.

Ramachandran plots generated with *PROCHECK* (Laskowski, 1993) indicate that the model exhibits good stereochemistry, with 89.8% of the residues in the most favoured regions and 10.2% in additionally allowed regions. Accessible surface-area calculations were performed using the *CCP*4 program *AREAIMOL*, leaving the probe solvent-

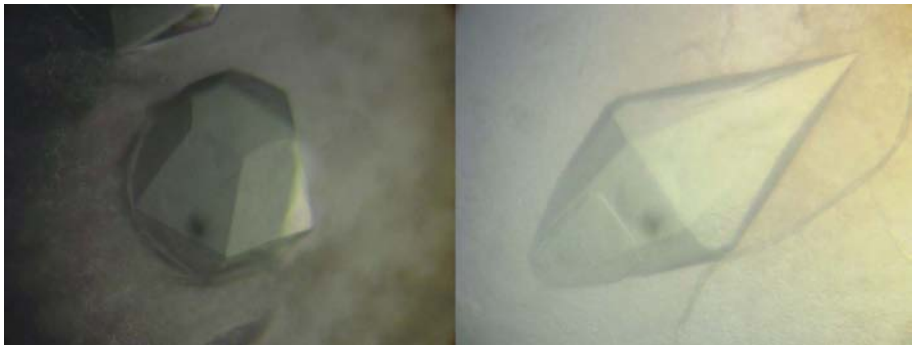

Figure 1
Pictures of *E. coli* wt-R2 crystals obtained with the new ammonium sulfate-based crystallization condition. The maximum length of the crystal shown on the right is 1 mm.

molecule radius at the default value of 1.4 Å (Collaborative Computational Project, Number 4, 1994). Crystal contacts were analyzed with the *CCP*4 program *CONTACT* using a 3.5 Å cutoff radius (Collaborative Computational Project, Number 4, 1994). Superpositions were performed with *LSQMAN* (Kleywegt & Jones, 1994) and figures were generated using *PyMOL* (DeLano, 2002).

3. Results and discussion

3.1. Relation to previous crystallization conditions

Like the very first crystallization report on *E. coli* wt-R2 in 1984 (Joelson *et al.*, 1984), the new crystal form is based on the precipitating agent ammonium sulfate. However, the shape of the crystals, their space group, unit cell and diffraction quality differ. The first R2 crystals were described as

> rectangular plates stuck together at one end in the form of a water wheel of an old Mississippi steamer

(Joelson *et al.*, 1984). Preliminary crystallographic data suggested an orthorhombic space group with unit-cell parameters $a = 58$, $b = 73$, $c = 205$ Å, but this crystal form was not useful for structure determination owing to streaks in the diffraction pattern (Nordlund *et al.*, 1989). The most obvious difference between that solution and the current condition is the presence of 100 m*M* $MgCl_2$, but there is no density for Mg^{II} ions that would explain a different packing in our new crystal form.

The crystallization condition widely employed for R2 structural studies is a precipitant containing 20% PEG 4000, 0.2 *M* NaCl, 0.3% dioxane, 50 m*M* MES pH 6.0 and 1 m*M* EMTS (Nordlund *et al.*, 1989). These crystals belong to space group $P2_12_12_1$ and have unit-cell parameters $a = 74$, $b = 86$, $c = 116$ Å. The crystals, which diffract to as high as 1.4 Å resolution (Högbom *et al.*, 2003), resemble rectangular cuvettes and typically have a large central cavity. Glycerol (20–25%) is typically used as a cryoprotecting agent. Interestingly, 1 m*M* EMTS is crucial for the diffraction quality of these R2 crystals. Without EMTS, a different poorly diffracting crystal form is obtained, also belonging to space group $P2_12_12_1$, but with significantly longer unit-cell parameters of $a = 58$, $b = 74$, $c = 355$ Å (Nordlund *et al.*, 1989). Although EMTS binds to the very same cysteine residues in our crystal form, it does not influence the diffraction quality or unit-cell parameters. Another alternative R2 crystallization condition was identified in 1998 (Tong *et al.*, 1998). Hexagonal crystals were grown from drops containing 50 m*M* Tris pH 7.6 and 5% glycerol equilibrated against a reservoir containing 80% saturated NaCl. The space group is $P6_1$, with unit-cell parameters $a = b = 140$, $c = 111$ Å. Glycerol (30%) is also used as a cryoprotectant for this crystal form.

Below, we compare the Mn^{II}-loaded structure obtained from the new crystal form (PDB code 2alx) with structures of wt-R2 obtained from the other two crystallization conditions. Representative examples of wt-R2 structures based on the PEG crystallization condition are the 1.4 Å resolution structure (PDB code 1mxr; Högbom *et al.*, 2003) and an Mn^{II}-substituted variant determined to 2.5 Å resolution (PDB code 1mrr; Atta *et al.*, 1992). The 2.8 Å resolution wt-R2 structure determined from the saturated NaCl condition (PDB code 1av8; Tong *et al.*, 1998) will also be discussed.

3.2. Description of the structure

The final model obtained from the new crystal form consists of one wt-R2 monomer per asymmetric unit. The physiological dimer is generated by a twofold crystallographic symmetry axis. In contrast, all other crystal structures of *E. coli* R2 contain one R2 dimer in the asymmetric unit. Only the structures of mouse R2 in space group $C222_1$ (Kauppi *et al.*, 1996) and *Chlamydia trachomatis* R2 in space group $P4_32_12$ (Högbom *et al.*, 2004) contain one R2 monomer per asymmetric unit. The overall protein fold is the same as reported previously. The R2 dimer is heart-shaped, with a β-hairpin at the tip and an α-helical core. Each monomer has eight long α-helices, three shorter capping α-helices and one 3_{10}-helix at the C-terminus. A superposition of the final model with monomer *A* from structures 1mxr and 1av8 gives root-mean-square deviations for the C^α atoms of 0.5 and 0.4 Å, respectively. The corresponding values for monomer *B* of 1mxr and 1av8 are 0.4 and 0.4 Å. These values fall within the coordinate error of 0.4 Å, estimated by a Luzzati plot, for the 2.6 Å resolution 2alx structure, suggesting that the structures are essentially identical. The dimer interface is also very similar. The surface areas occluded upon dimerization are 6202 $Å^2$ for 2alx, 6149 $Å^2$ for 1mxr and 6107 $Å^2$ for 1av8.

An overlay of the C^α traces for monomer *A* from all three models is shown in Fig. 2. The only significant deviation is observed for residues 147–152 in monomer *A* of model 1mxr, which are shifted with respect to structures 2alx and 1av8. In particular, the C^α position of residue Glu151 is shifted by ~4 Å in both monomers of 1mxr compared with 2alx and 1av8. Residues 147–152 are located on the short capping helix

α2b and form the connection to helix αD. In the other two structures, 2alx and 1av8, this region has α-helical character and is an extension of helix αD. It is possible that the distortion of helix αD is only detectable at higher resolution, but lower resolution structures also derived from the PEG-based crystal form such as 1mrr to 2.5 Å (Atta *et al.*, 1992) and 1piy to 1.7 Å (Voegtli *et al.*, 2003) also show the distortion in monomer *B*. In monomer *A*, however, helix α2b is modelled similarly to those in 2alx and 1av8. A careful inspection of this helix in our model with simulated-annealing omit maps indicates that at 2.6 Å resolution there is no apparent distortion in helix αD. The difference between the PEG-based crystal form represented by 1mxr and the other two crystal forms is partly explained by crystal contacts. In monomer *B* of 1mxr, residues Glu144*B* and Glu151*B* form salt bridges with Asn131*A* and Arg57*B*, respectively. Surprisingly, the same residues in monomer *A* of 1mxr are not involved in crystal contacts, but the same helical distortion is modeled.

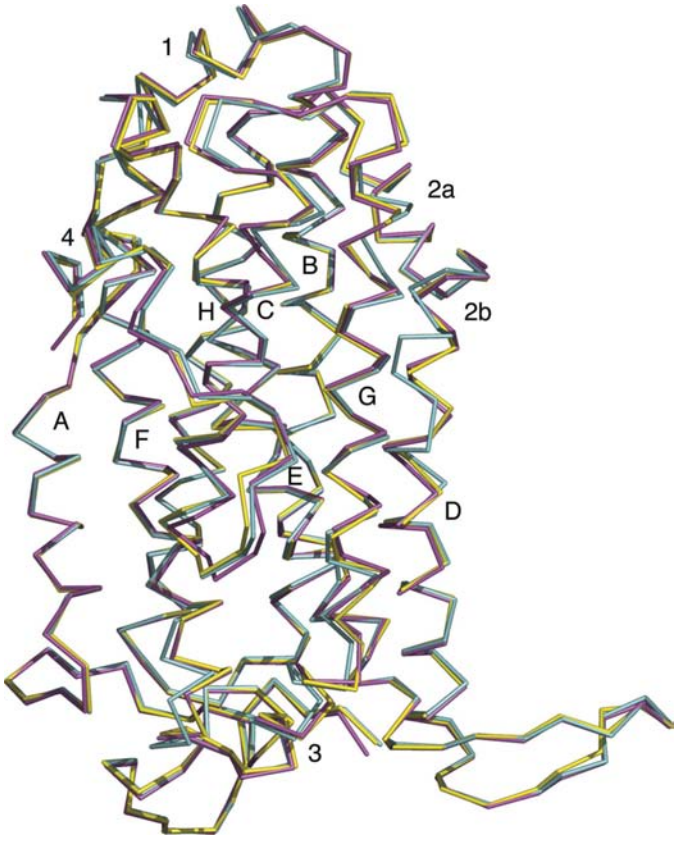

Figure 2
Superposition of the C^{α} traces of wt-R2 determined from three different crystal forms with PDB codes 2alx (yellow), 1mxr (cyan) and 1av8 (magenta).

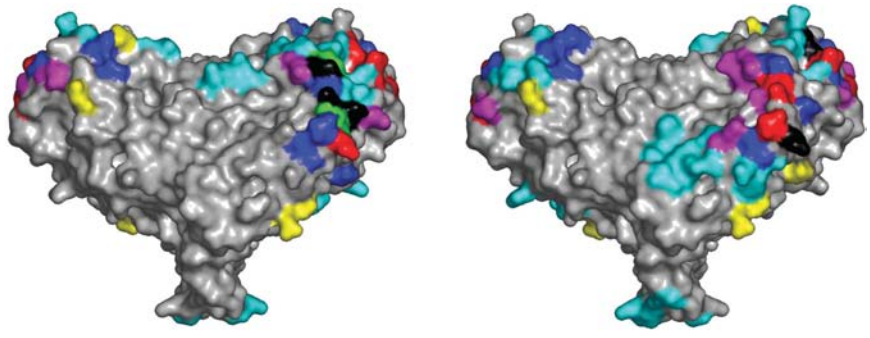

Figure 3
Surface representation of the R2 dimer with residues involved in crystal contacts highlighted. Crystal contacts occurring only in one crystal form are colored blue for 2alx, cyan for 1mxr and magenta for 1av8. Crystal contacts present in two of the three crystal forms are colored yellow for 2alx and 1mxr, red for 2alx and 1av8 and green for 1mxr and 1av8. Finally, residues that form crystal contacts in all three crystal forms are black. Two different views of the structure related by a 180° rotation are displayed.

The final refined model from all three different crystal forms is limited to residues 1–339/340, with the C-terminal 35 or 36 residues not visible in the electron density. These residues are crucial for interaction with the R1 subunit (Climent *et al.*, 1992) and, as demonstrated by NMR spectroscopy for mouse RNR, only become ordered upon complex formation between the R1 and R2 subunits (Lycksell *et al.*, 1994). Crystallographic insight into this region has only been obtained in two cases. Firstly, successful crystallization of *E. coli* R1 required addition of a 20-residue polypeptide comprising residues 356–375 of the R2 C-terminus (Uhlin & Eklund, 1994). Secondly, the structure of the yeast Rnr4 homodimer, a non-reactive homolog of R2 (Ge *et al.*, 2001), revealed ten additional C-terminal residues ordered by crystal-packing interactions (Sommerhalter *et al.*, 2004).

3.3. Crystal packing

In each crystal form, different amino acids participate in crystal contacts (Fig. 3). In the new crystal form, 16 residues are involved, excluding those that form the dimer interface. Owing to crystallographic symmetry, both monomers have identical crystal contacts. In contrast, structures 1mxr and 1av8 have slightly different packing interactions in the two monomers. For both monomers *A* and *B* of 1mxr, 26 residues form lattice contacts. Contacts in structure 1av8 include 15 residues from monomer *A* and 13 residues from monomer *B*. In all three structures, most residues involved in crystal contacts are derived from helices α1, αB, αG and αH, the loop between helices αG and αH and residues 328–334 in the unstructured C-terminal region. The β-hairpin tip of the heart shape forms only crystal contacts in structure 1mxr. In the other two crystal forms, this region faces a solvent channel. Based on a Matthews coefficient analysis (Kantardjieff & Rupp, 2003), solvent contents of 57, 40 and 66% are calculated for 2alx, 1mxr and 1av8, respectively. The considerably lower solvent content and higher number of crystal contacts for the PEG-based crystal form represented by 1mxr are correlated with its superior diffraction quality.

3.4. R2 metal site

The presence of 10–50 m*M* $CoCl_2$ or $MnCl_2$ in the crystallization solution results

in full occupancy of the dinuclear metal center in the asymmetric unit [data not shown for the Co^{II} crystals]. Both Mn^{II} positions have occupancy values of 1.0 with reasonable *B* factors and the active-site electron density is well defined. Since the two monomers are related by twofold crystallographic symmetry, all four metal positions in the R2 dimer are fully occupied. Both Co^{II} and Mn^{II} have been employed previously as models or spectroscopic probes for the Fe^{II} ions (Atta *et al.*, 1992; Strand *et al.*, 2002). Recent solution titrations of Mn^{II} and Fe^{II} into R2 monitored by EPR quantitation suggest that metal loading occurs initially in only one monomer. Loading of the second monomer then requires the reaction of Fe^{II} and O_2 in the first monomer (Pierce *et al.*, 2003; Pierce & Hendrich, 2005). On the basis of these data, Hendrich and coworkers have proposed a model for R2 metal incorporation that involves allosteric interactions between the two monomers. This phenomenon is not observed in solution studies in the presence of glycerol (Atta *et al.*, 1992; Pierce *et al.*, 2003). In the current structure all four metal sites are occupied even in the absence of glycerol, as required by the crystallographic symmetry. The loading mechanism could be sensitive to other components of the crystallization solution. For the PEG-based crystal form, full Mn^{II} occupancy was accomplished by soaking apo crystals in 5 m*M* $MnCl_2$ (Atta *et al.*, 1992; Högbom *et al.*, 2001). In this case, the crystal packing might trap the protein in a conformation that does not require allosteric changes to bind four metal ions.

The coordination environment of the two Mn^{II} ions is depicted in Fig. 4. At 2.6 Å resolution, detailed metrical parameters cannot be reported, but the overall geometry is similar to that observed in dimanganese(II) structures from the PEG-based crystal form (Atta *et al.*, 1992; Högbom *et al.*, 2001). The Mn—Mn distance is approximately 3.8 Å, which is somewhat longer than the 3.6 Å observed in the previous structures. Electron density previously attributed to an exogenous solvent ligand was not detected. This difference reduces the coordination number of the Mn^{II} ion coordinated by His241 to four. These discrepancies might be a consequence of the slightly lower resolution of our data set, 2.6 Å, compared with 2.5 Å for 1MRR. Considering the versatility of the diiron(II) center with respect to different metal-loading protocols (Voegtli *et al.*, 2003), it is also possible that the new crystal form changes the active-site geometry of the Mn^{II}-substituted variant.

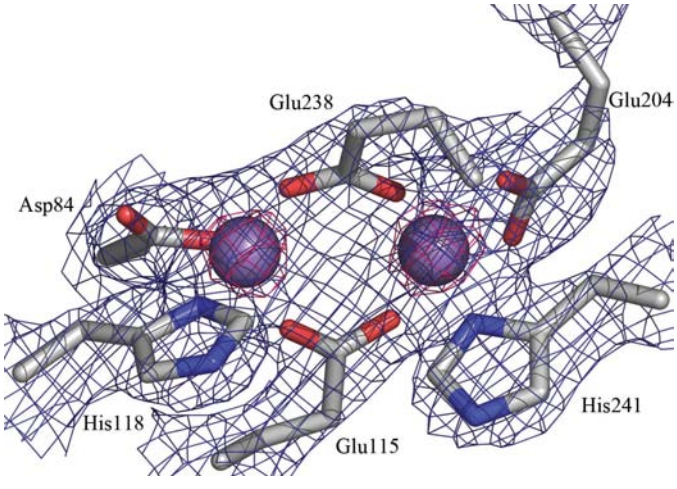

Figure 4
The active site of 2alx with the $2F_o - F_c$ map superimposed (blue, contoured at 1.5σ; pink, contoured at 8σ). The Mn^{II} ions are shown as magenta spheres.

4. Conclusions

A new crystal form of the *E. coli* wt-R2 dimer was obtained and the structure of the Mn^{II}-substituted form determined to 2.6 Å resolution. This is the first *E. coli* R2 structure with one monomer, rather than the physiological dimer, in the asymmetric unit. The structure corroborates the overall fold of previous models, with the exception of a small deviation in helix α2b. In contrast to solution data, which suggest a sequential metal-loading mechanism, all four metal-binding sites are fully occupied. Optimization of this crystal form to obtain higher resolution could provide new insights into the active-site structure and provides an opportunity to conduct experiments in the crystalline state in the absence of PEG and glycerol.

This work was supported by NIH grant GM58518. DND-CAT is supported by E. I. DuPont de Nemours & Co., the Dow Chemical Company, the US National Science Foundation through Grant DMR-9304725 and the State of Illinois through the Department of Commerce and the Board of Higher Education Grant IBHE HECA NWU 96.

References

Andersson, M. E., Högbom, M., Rinaldo-Matthis, A., Andersson, K. K., Sjöberg, B.-M. & Nordlund, P. (1999). *J. Am. Chem. Soc.* **121**, 2346–2352.
Atta, M., Nordlund, P., Aberg, A., Eklund, H. & Fontecave, M. (1992). *J. Biol. Chem.* **267**, 20682–20688.
Brünger, A. T., Adams, P. D., Clore, G. M., DeLano, W. L., Gros, P., Grosse-Kunstleve, R. W., Jiang, J.-S., Kuszewski, J., Nilges, M., Pannu, N. S., Read, R. J., Rice, L. M., Simonson, T. & Warren, G. L. (1998). *Acta Cryst.* D**54**, 905–921.
Climent, I., Sjöberg, B.-M. & Huang, C. Y. (1992). *Biochemistry*, **31**, 4801–4807.
Collaborative Computational Project, Number 4 (1994). *Acta Cryst.* D**50**, 760–763.
DeLano, W. L. (2002). *The PyMOL Molecular Graphics System.* San Carlos, CA, USA: DeLano Scientific.
Eklund, H., Uhlin, U., Färnegårdh, M., Logan, D. T. & Nordlund, P. (2001). *Prog. Biophys. Mol. Biol.* **77**, 177–268.
Ge, J., Perlstein, D. L., Nguyen, H. H., Bar, G., Griffin, R. G. & Stubbe, J. (2001). *Proc. Natl Acad. Sci. USA*, **98**, 10067–10072.
Högbom, M., Andersson, M. E. & Nordlund, P. (2001). *J. Biol. Inorg. Chem.* **6**, 315–323.
Högbom, M., Galander, M., Andersson, M., Kolberg, M., Hofbauer, W., Lassmann, G., Nordlund, P. & Lendzian, F. (2003). *Proc. Natl Acad. Sci. USA*, **100**, 3209–3214.
Högbom, M., Stenmark, P., Voevodskaya, N., McClarty, G., Gräslund, A. & Nordlund, P. (2004). *Science*, **305**, 245–248.
Joelson, T., Uhlin, U., Eklund, H., Sjoberg, B. M., Hahne, S. & Karlsson, M. (1984). *J. Biol. Chem.* **259**, 9076–9077.
Kabsch, W. (1993). *J. Appl. Cryst.* **26**, 795–800.

Kantardjieff, K. A. & Rupp, B. (2003). *Protein Sci.* **12**, 1865–1871.
Kauppi, B., Nielsen, B. B., Ramaswamy, S., Larsen, I. K., Thelander, M., Thelander, L. & Eklund, H. (1996). *J. Mol. Biol.* **262**, 706–720.
Kleywegt, G. J. & Jones, T. A. (1994). *Jnt CCP4/ESF–EACBM Newsl. Protein Crystallogr.* **31**, 9–14.
Laskowski, R. A. (1993). *J. Appl. Cryst.* **26**, 283–291.
Logan, D. T., Su, X.-D., Åberg, A., Regnström, K., Hajdu, J., Eklund, H. & Nordlund, P. (1996). *Structure*, **4**, 1053–1064.
Lycksell, P. O., Ingemarson, R., Davis, R., Gräslund, A. & Thelander, L. (1994). *Biochemistry*, **33**, 2838–2842.
McRee, D. E. (1999). *J. Struct. Biol.* **125**, 156–165.
Moënne-Loccoz, P., Baldwin, J., Ley, B. A., Loehr, T. M. & Bollinger, J. M. Jr (1998). *Biochemistry*, **37**, 14659–14663.
Murshudov, G. N., Vagin, A. A. & Dodson, E. J. (1997). *Acta Cryst.* D**53**, 240–255.
Noodleman, L., Lovell, T., Han, W. G., Li, J. & Himo, F. (2004). *Chem. Rev.* **104**, 459–508.
Nordlund, P. & Eklund, H. (1993). *J. Mol. Biol.* **231**, 123–164.
Nordlund, P., Sjöberg, B.-M. & Eklund, H. (1990). *Nature (London)*, **345**, 593–598.
Nordlund, P., Uhlin, U., Westergren, C., Joelson, T., Sjöberg, B.-M. & Eklund, H. (1989). *FEBS Lett.* **258**, 251–254.
Pierce, B. S., Elgren, T. E. & Hendrich, M. P. (2003). *J. Am. Chem. Soc.* **125**, 8748–8759.
Pierce, B. S. & Hendrich, M. P. (2005). *J. Am. Chem. Soc.* **127**, 3613–3623.
Powell, H. R. (1999). *Acta Cryst.* D**55**, 1690–1695.
Pulver, S. C., Tong, W. H., Bollinger, J. M. Jr, Stubbe, J. & Solomon, E. I. (1995). *J. Am. Chem. Soc.* **117**, 12664–12678.
Reichard, P. (1993). *Science*, **260**, 1773–1777.
Rubinson, K. A., Ladner, J. E., Tordova, M. & Gilliland, G. L. (2000). *Acta Cryst.* D**56**, 996–1001.
Sjöberg, B.-M. (1997). *Struct. Bonding*, **88**, 139–173.
Sommerhalter, M., Lieberman, R. L. & Rosenzweig, A. C. (2005). *Inorg. Chem.* **44**, 770–778.
Sommerhalter, M., Voegtli, W. C., Perlstein, D. L., Ge, J., Stubbe, J. & Rosenzweig, A. C. (2004). *Biochemistry*, **43**, 7736–7742.
Strand, K. R., Karlsen, S. & Andersson, K. K. (2002). *J. Biol. Chem.* **277**, 34229–34238.
Stubbe, J. & van der Donk, W. A. (1998). *Chem. Rev.* **98**, 705–762.
Tong, W., Burdi, D., Riggs-Gelasco, P., Chen, S., Edmondson, D., Huynh, B. H., Stubbe, J., Han, S., Arvai, A. & Tainer, J. (1998). *Biochemistry*, **37**, 5840–5848.
Tshuva, E. Y. & Lippard, S. J. (2004). *Chem. Rev.* **104**, 987–1012.
Uhlin, U. & Eklund, H. (1994). *Nature (London)*, **370**, 533–539.
Vagin, A. & Teplyakov, A. (1997). *J. Appl. Cryst.* **30**, 1022–1025.
Voegtli, W. C., Khidekel, N., Baldwin, J., Ley, B. A., Bollinger, J. M. Jr & Rosenzweig, A. C. (2000). *J. Am. Chem. Soc.* **122**, 3255–3261.
Voegtli, W. C., Sommerhalter, M., Saleh, L., Baldwin, J., Bollinger, J. M. Jr & Rosenzweig, A. C. (2003). *J. Am. Chem. Soc.* **125**, 15822–15830.